

Antibacterial Antimicrobial Peptide Grafted HA/SF/Alg Wound Dressing Containing AIEgens for Infected Wound Treating

Yize Lin,[#] Yan Tan,[#] Rong Deng, Li Gong, Xiaoshan Feng, Zhongqi Cai, Yanxian He, Longbao Feng, Biao Cheng,^{*} and Yi Chen^{*}



Cite This: *ACS Omega* 2024, 9, 23499–23511



Read Online

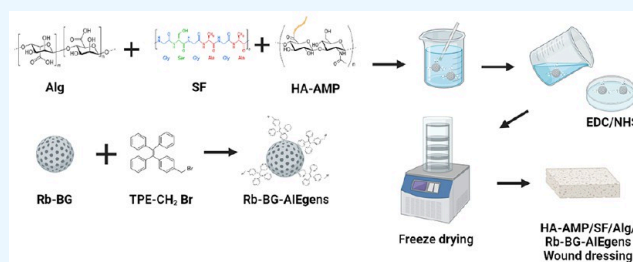
ACCESS |

Metrics & More

Article Recommendations

Supporting Information

ABSTRACT: Chronic wounds are characterized with excessive biofluid and persistent infection. Therefore, there is an urgent desire to develop a multifunctional wound dressing that can meet the extreme requirements including effective antibacterial and powerful wound microenvironment regulation and protection function to promote wounds heal quickly. In this study, a multifunctional composite dressing (HA-AMP/SF/Alg/Rb-BG-AIEgens) was synthesized by combining a mesoporous bioactive glass framework loaded with AIEgens (Rb-BG-AIEgens) with cross-linked antimicrobial peptide grafted hyaluronic acid (HA-AMP), sodium alginate (Alg), and silk fibroin (SF). It is important to note that the Rb-BG-AIEgens can achieve real-time and sensitive bacterial detection. HA-AMP can achieve broad spectrum antibacterial and avoid the residue of drug-resistant bacteria. The HA-AMP/SF/Alg/Rb-BG-AIEgens dressing can up-regulate related proliferative proteins, thereby promoting regeneration of tissue and the rapid healing of chronic wounds. With good biocompatibility and antibacterial ability, HA-AMP/SF/Alg/Rb-BG-AIEgens dressing has great potential to become a next generation wound dressing for clinical biological fluid management and chronic bacterial infection treatment.



1. INTRODUCTION

Wound infection is a core problem in the process of wound healing, it can delay wound healing¹ and even lead to systemic infection or organ dysfunction.² After skin is damaged, the ability to resist bacteria is greatly reduced, leading to long-term chronic inflammation.³ Therefore, the development of multifunctional dressings with simultaneous bacterial monitoring and rapid antibacterial, anti-inflammatory, and exudate adsorption would contribute to the rapid healing of chronic wounds.⁴

Traditional wound dressings,⁵ including gauze or bandages, only have basic hemostasis functions without avoiding the various risks of wound deterioration.⁶ At present, there are many kinds of therapeutic dressings, such as microfibers,⁷ hydrogels,⁸ sponges, and films, etc.⁹ Among them, spongy dressings¹⁰ are formed by cross-linking different polymers, and the porous structure of spongy dressings are conducive to absorb a large amount of tissue exudates, while maintaining a moisturizing effect on the wound surface, which has advantages in wound healing.¹¹

Hyaluronic acid (HA),¹² a biodegradable skin extracellular matrix (ECM) compound, is considered as a major player in the tissue regeneration process.¹³ HA-based wound dressings have been developed for many respects with good surface hydrophilicity.¹⁴ HA polymer networks can be quickly formed by cross-linking through ion exchange processes.¹⁵ Silk fibroin

(SF)¹⁶ is the fibrous protein extracted from silk produced by *Bombyx mori*.¹⁷ SF connected the pore structure inside and outside of the polymer networks,¹⁸ regulating the physical support, which helps the cell to carry out the exchange of oxygen, nutrients, and growth factors.¹⁹ Moreover, it provides attachment sites and selectively interacts with cells, making SF-based polymer networks highly appealing as cell scaffolds for muscle tissue regeneration.²⁰ Sodium alginate (Alg), typically sourced from brown algae and bacteria,²¹ is a linear anionic polysaccharide known for its rapid solubility in aqueous solutions or high-humidity environments.²² Furthermore, its hemostatic properties, promotion of cell migration and angiogenesis, as well as its high moisture retention and intrinsic biodegradability, make it a valuable component in tissue dressings.^{23,24}

Antibiotics are often added to dressings for the treatment of wound infections, but their low bioavailability and susceptibility to drug resistance have limited the development of wound repair.²⁵ Antimicrobial peptide (AMP)²⁶ is a highly

Received: January 19, 2024

Revised: April 27, 2024

Accepted: May 13, 2024

Published: May 21, 2024



effective antibacterial agent, which has the advantages of broad-spectrum antibacterial activity²⁷ and rapid detection of targets.²⁸ In recent years, AMP has become an ideal alternative to fight drug-resistant bacterial infections due to its various advantages of strong designability, versatility and low cost.^{29,30}

In the face of the challenges posed by bacterial infections and drug resistance,³¹ achieving sensitive bacterial detection and monitoring the effectiveness of antibacterial treatments are the basis for accurate treatment of bacterial infections.³² Aggregation-induced emission (AIE) luminogens (AIEgens)³³ are fluorescent probes which can be responsive to the bacterial microenvironment and enable accurate bacterial targeting, tracking, sterilization, and repair.³⁴ Bioactive glass is an inorganic material exhibiting biological activity, characterized by exceptional biocompatibility and bioactivity. It can engage in chemical interactions with biological tissues, thereby facilitating tissue regeneration and wound healing.³⁵ Among various metallic ions, rubidium ions (Rb⁺) demonstrate favorable antibacterial activity by disrupting the membrane potential of bacteria. Additionally, Rb-doped bioactive glass has been proven to enhance wound healing.³⁶

Herein, we designed a bacterial responsive antimicrobial dressing by grafting HA-AMP to functionalized SF/Alg sponge and using AIEgens-carrying mesoporous bioactive glass framework (Rb-BG-AIEgens) as cross-linking agents for liquid absorption and antibacterial to promote wound healing. To be specific, HA-AMP, SF, and Alg were first cross-linked via an amide reaction to form a macroporous sponge network (HA-AMP/SF/Alg). Then, the macroporous sponge HA-AMP/SF/Alg was combined with Rb-BG-AIEgens to form a composite sponge HA-AMP/SF/Alg/Rb-BG-AIEgens with antibacterial and AIEgens fluorescence tracking ability. On the basis of the urgent clinical need for real-time and sensitive bacterial detection and in situ killing, composite HA-AMP/SF/Alg/Rb-BG-AIEgens dressing can build an integrated system of "monitoring and killing bacteria" for the microenvironment of bacterial infection sites, which has broad application prospects in the field of diagnosis and treatment of bacterial infectious diseases.

2. MATERIALS AND METHODS

2.1. Materials and Reagents. Poly(ethylene oxide)-poly(propylene oxide)-poly(ethylene oxide) triblock copolymer (P123), antimicrobial peptide (KRWKWWRRRC), dimethyl sulfoxide (DMSO), rubidium chloride, sodium carbonate, tetraethyl silicate, and triethyl phosphate (TEP) were purchased from Aladdin (Shanghai, China). Sodium alginate acid, 1-ethyl-(3-(dimethylamino)propyl) carbamide diimide (EDC), and *N*-hydroxysuccinimide (NHS) were purchased from Macklin (Shanghai, China). Bromomethyl tetraphenylethylene (TPE-CH₂ Br) were obtained from AIEGEN Biotech., Ltd. Cell counting kit-8 (CCK-8) and BCA protein assay kit were acquired from Beyotime Biotechnology (Shanghai, China). Hyaluronic acid was purchased from Shanghai yuanye Bio-Technology Co., Ltd. (Shanghai, China). LIVE/DEAD bacterial viability kit was bought from Thermo Fisher Scientific Co., LTD (Shanghai, China). Dulbecco's modified Eagle's medium (DMEM), fetal bovine serum (FBS), penicillin/streptomycin and trypsin were purchased from Gibco Corporation (Shanghai, China). All reagents were analytical reagent grade.

2.2. Synthesis of AIEgens-Loaded Mesoporous Bioactive Glass (Rb-BG-AIEgens). AIEgens-loaded mesoporous

bioactive glass was prepared by the injection method. Briefly, template agent P123 (8 g), calcium nitrate (1.86 g), triethyl phosphate (1.44 g), and tetraethyl silicate (14 mL) were dissolved in ethanol (150 mL) and homogeneous mixing as solution A. Solution B was obtained by dissolving rubidium chloride (0.048 g/mL) in 10 mL of deionized water. The molar ratio of the four elements of rubidium, calcium, phosphorus, and silicon was 5:10:5:80, separately. The solution was quickly added to the solution B and vigorously stirred for 24 h at room temperature to obtain mixed gel. Finally, the polyurethane sponge was soaked in the obtained gel for 10 min and blow dried for 5 min, repeated for four times. After the sponge was completely dried and then burned at 700 °C for 8 h, bioactive glass drug carrier containing rubidium mesoporous (Rb-BG) was obtained. Rb-BG-AIEgens was synthesized by mixing AIEgens (0.1 g/mL) solution with Rb-BG (0.2 g/mL) and stirred for 24 h at room temperature. The obtained solution was centrifuged (6000g, 10 min, 4 °C) and dried to collect the Rb-BG-AIEgens powder.

2.3. Synthesis of HA-AMP. The 500 mg of antimicrobial peptide (AMP) were dissolved in 200 mL of hyaluronic acid solution (4 mg/mL) and sonicated for 4 h. 750 mg of EDC and 660 mg of 1-hydroxybenzotriazole (HoBt) were dissolved in 10 mL DMSO/H₂O (1:1) solution. NaOH and HCl solution were used to adjust the pH of the above solution to 4.75. After reaction for 4 h, the reaction was finished by changing the pH to 7.0. The reaction mixture was placed in deionized water for dialysis for 1 day (molecular weight cut off, MWCO = 8000 Da). The pure HA-AMP powder was obtained after lyophilization.

2.4. Preparation of Silk Fibroin (SF) Solution. A 10-g portion of silkworm cocoon was boiled in 2 L Na₂CO₃ (0.5 mM) solution for degumming. The SF was washed three times repeatedly using distilled water. The pure silk fibroin was obtained by drying in an oven. Then, 10 g of silk fibroin was dissolved in 80 mL of lithium bromide (9.3 M). Under 60 °C water base, 0.48 g of NaOH was added for 1 h with continuous stirring. One mL HCl was added to neutralize the unreacted NaOH and continue the reaction for 3 h. The mix solution was dialyzed against deionized water for 48 h (MWCO = 12 000 Da). The pure SF was obtained by lyophilization.

2.5. Preparation of Wound Dressing (HA-AMP/SF/Alg/Rb-BG-AIEgens). 3% SF, 3% Alg, and 1% HA-AMP solutions were mixed at a ratio of 1:1:1 obtained SF/Alg/HA mixing solution. And then, the Rb-BG-AIEgens (1 mg/mL) was added to the above SF/Alg/HA mixed solution. The well-mixed solution was added into a 48-well plate (600 μL/per well) and lyophilized for use. EDC (9.2 mg/mL) and NHS (2.8 mg/mL) ethanol solution was added for cross-linking for 48 h. After cross-linking, the solutions were washed several times with gradient concentration of ethanol solution to remove residual EDC and NHS. Afterward, different ratios of HA-AMP/SF/Alg/Rb-BG-AIEgens were obtained after lyophilization.

2.6. Chemical Construction and Morphology of Wound Dressing. **2.6.1. Chemical Construction of HA-AMP.** The chemical structure of HA and HA-AMP were characterized by ¹H NMR spectra (Inova-500M, Varian Co. Ltd., U.S.A.). The samples were determined by NMR spectrometer at room temperature, and the spectra were analyzed by MestReNova software. The Fourier transform infrared (FTIR) was carried out to determine the bonding nature of the synthesized HA and HA-AMP. The samples were

recorded on FT-IR spectrometer (VERTEX70, Germany). The scanning range was from 4000 to 500 cm^{-1} .

2.6.2. SEM Observation. The microstructures of the Rb-BG, Rb-BG-AIEgens, HA/SF/Alg, HA-AMP/SF/Alg, and HA-AMP/SF/Alg/Rb-BG-AIEgens were characterized by scanning electron microscope (SEM, S-3400, Hitachi, Japan). Before examination, the samples were freeze-dried. The dried hydrogels were cut out, and the surface of the cross-section was observed by SEM analysis. The average aperture was calculated using Nano measure software.

2.7. Fluorescence Spectra of Rb-BG-AIEgens. The fluorescence spectra recorded by fluorospectro photometer (UV1800, Shimadzu). The Rb-BG-AIEgens aqueous solutions with concentration gradients of 1000 $\mu\text{g/mL}$, 800 $\mu\text{g/mL}$, 600 $\mu\text{g/mL}$, 400 $\mu\text{g/mL}$, 200 $\mu\text{g/mL}$, 100 $\mu\text{g/mL}$, 50 $\mu\text{g/mL}$, 25 $\mu\text{g/mL}$, 10 $\mu\text{g/mL}$, and 0 $\mu\text{g/mL}$ were prepared in gradient. The excitation wavelength was 360 nm and the range of emission wavelength was from 200 to 800 nm.

2.8. Physical Properties of Wound Dressings.

2.8.1. Water Vapor Transmission Rate (WVTR) Tests. We tested the water vapor transmission rate of Alg/SF/HA, Alg/SF/HA-AMP, HA-AMP/SF/Alg/Rb-BG-AIEgens by the following method. Briefly, the simulated wound fluid was added to a moisture permeable cup with a height of 5 cm, and the bottle was sealed with specimens. Then it was placed in a constant temperature and the humidity difference was maintained between the two sides of the sample. The weight measurements were made over 6 h when reached at steady-state conditions. The water vapor transmission rate was calculated with the following the formula:

$$\text{WVTR} = (W_0 - W_1) \times 24 / (s \times t)$$

where W_0 represents the initial mass of the system (g), W_1 represents the final mass of the system (g), s represents the area (cm^2), t represents the test time, and the unit of WVTR is ($\text{g} \cdot 24 \text{ h}^{-1} \cdot \text{m}^2$).

2.8.2. Swelling Performance Tests. For the swelling behavior of Alg/SF/HA, Alg/SF/HA-AMP, and HA-AMP/SF/Alg/Rb-BG-AIEgens wound dressing in water. The samples were first weighted (m_0) and calculated the area (s) of the dressing support. The samples were immersed in deionized water at room temperature, and then they were removed and weighed at different times (m_t). The water absorption ratio (W) was calculated as above:

$$W = (m_t - m_0) / s$$

2.8.3. Porosity Test. The porosity of Alg/SF/HA, Alg/SF/HA-AMP, and HA-AMP/SF/Alg/Rb-BG-AIEgens were measured by the following methods. A certain amount of ethanol was used to infiltrate the sample, and the liquid volume was used as V_1 . The container was evacuated for 1 h to remove all air in the sample holes, and the liquid volume at this time was recorded as V_2 . After sample removal, the volume of remaining ethanol was recorded as V_3 . The porosity M (%) was calculated according to the formula:

$$M = (V_1 - V_3) / (V_2 - V_3)$$

2.8.4. Degradation Performance. The dressing that reached swelling equilibrium was freeze-dried, weighed, and recorded as W_0 . The degradation behavior of wound dressings was evaluated in PBS environment containing 1000 U/mL lysozyme. The weight of the composite wound dressing was recorded after freeze-drying, W_t represents the mass of

dressings at a specific point in time. The degradation rate of wound dressing in vitro was calculated as follows:

$$\text{degradation ratio} = (W_0 - W_t) / W_0$$

2.8.5. In Vitro Mechanical Properties of HA/SF/Alg Dressing. The testing dressings were cut into rectangles measuring $75 \times 15 \text{ mm}^2$. Its thickness was measured using a thickness gauge under room temperature and 60% humidity conditions. Subsequently, its tensile mechanical properties were determined using a universal materials testing machine with the following parameters: a tensile speed of 10 mm/min, a grip distance of 65 mm, and a sample width of 15 mm. The Young's modulus, tensile strength, and elongation at break of the sample were directly obtained from the instrument.

2.9. In Vitro Antibacterial Test. **2.9.1. Bacterial Culture and Antibacterial Tests.** *Escherichia coli* (*E. coli*) and *Staphylococcus aureus* (*S. aureus*) were resuscitated and cultured to logarithmic growth phase. Then bacteria were collected by centrifugation and resuspended in saline to obtain a final concentration of 1×10^8 CFU/mL bacteria solution. The Rb-BG-AIEgens, Rb-BG-AIEgens/HA/SF/Alg, and HA-AMP/SF/Alg/Rb-BG-AIEgens wound dressings were disinfected by ultraviolet (UV) light for 24 h and then cocultured with bacterial suspension 37°C for 4 h. Sterile saline was used as the control group. The bacterial suspension after culturing was gradient diluted, coated on Luria–Bertani (LB) agar plates culturing for 24 h and counted.

2.9.2. Bacterial Live and Dead Fluorescent Staining. Bacteria cocultured with the wound dressing as described in section 2.9.1 were collected, and the bacterial precipitate was collected by centrifugation at 5000 rpm for 10 min. The bacteria were resuspended in 1 mL of normal saline, then 3 μL dead/live bacterial fluorescent staining reagent (Sytox Green Nucleic Acid Stain-9 (Syto-9): propidium iodide (PI) = 1:1) was added and stained in the dark for 15 min at room temperature. Then the bacteria were washed three times with phosphate buffered saline (PBS) to remove excess dye. The bacteria were observed and photographed by inverted fluorescence microscope. Syto-9 showed green fluorescence at an excitation/emission wavelength of 539/570–620 nm, and PI showed red fluorescence at an excitation/emission wavelength of 470/490–540 nm.

2.9.3. Scanning Electron Microscope. The cultured bacterial broth was removed and centrifuged (3000–5000 rpm/20 min), and the precipitate was removed and dispersed in PBS buffer containing 2.5% glutaraldehyde for 2 h for fixation. Several washes with PBS were used to remove residual organic fixative and finally dispersed in deionized water. A drop of 5 μL was applied to a single crystal silicon wafer, air-dried naturally, fixed, and sprayed with gold for 120 s before observing.

2.9.4. Biological Attack Resistance Test. Three different sewage samples were collected. Wound dressings were immersed in 10 mL of sewage samples and cultured at 37°C for 4 h. Then the dressings were taken out and sewage samples were continued incubation under 37°C for 24 h. The bacteria numbers were calculated by gradient diluted sewage samples, coated on LB agar plates culturing for 24 h and counted.

2.10. In Vitro Cytotoxicity and Cell Migration. **2.10.1. In Vitro Cytotoxicity.** The dressings were sterilized overnight by UV irradiation and added to DMEM complete medium at a mass ratio of 1:10. After 24 h of incubation, the

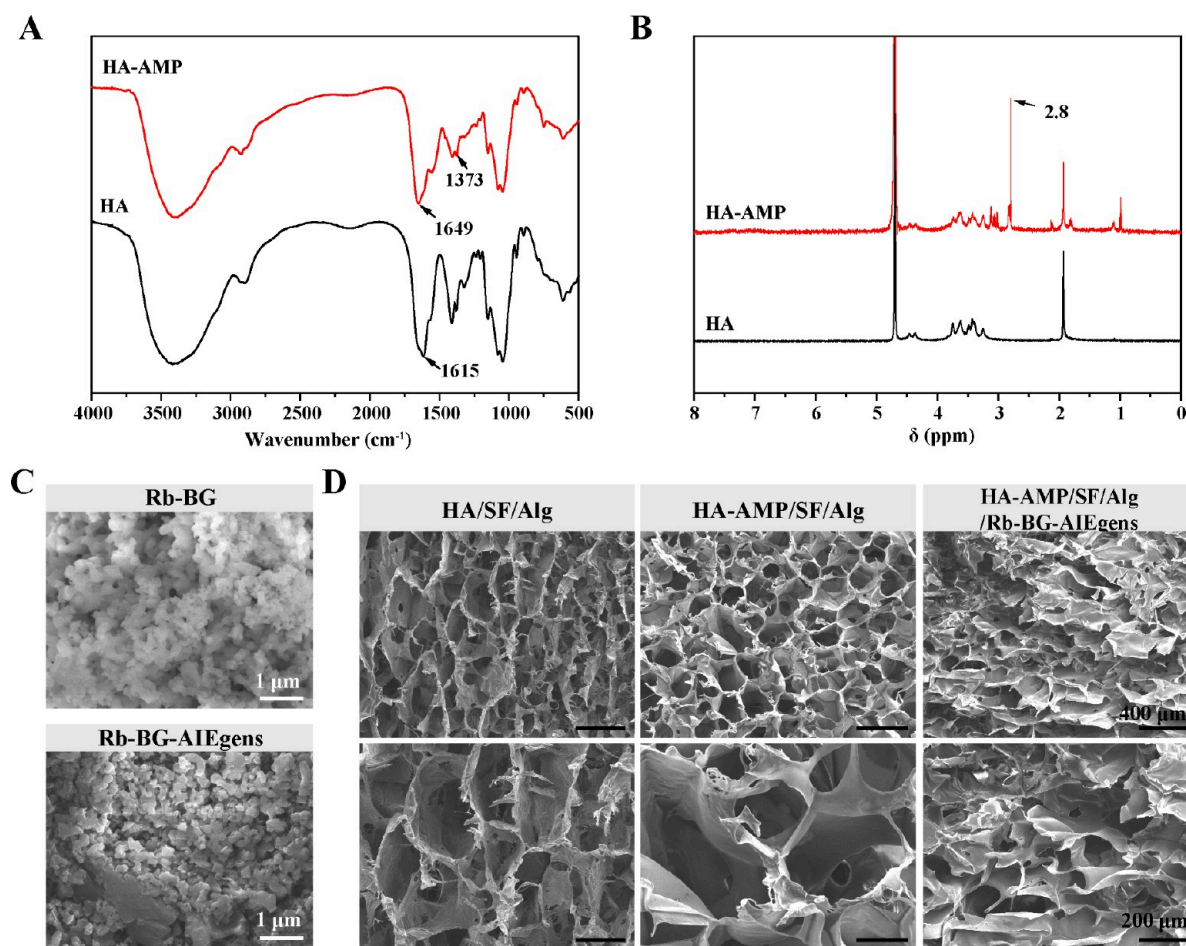


Figure 1. (A) FTIR and (B) ^1H NMR spectra of HA and HA-AMP; (C) SEM images of Rb-BG and Rb-BG-AIEgens; and (D) cross-sectional morphology of HA/SF/Alg, HA-AMP/SF/Alg, and HA-AMP/SF/Alg/Rb-BG-AIEgens wound dressings; scale bar = 1 μm .

supernatant was filtered with a sterile 0.22 μm filter and used as the extract liquid. To evaluate the cytotoxicity of composite wound dressing, 3T3 mouse fibroblast cells were used. Briefly, 3T3 cells were inoculated onto 96-well plates at a density of 1×10^4 per well. After overnight incubation, extract liquid of HA/SF/Alg, Rb-BG-AIEgens/H A/SF/Alg, and HA-AMP/SF/Alg/Rb-BG-AIEgens were incubated with the cells for 24 h. After that, the cells were washed with PBS and CCK-8 reagent was added and further incubated for 0.5 h. The absorbance of each well was measured on microplate reader (EPOCH2, China) at 450 nm. Cell survival rate was calculated by the following formula:

$$\text{cell survival rate (\%)} = \frac{(\text{OD}_{\text{experimental}} - \text{OD}_{\text{blank}}) / (\text{OD}_{\text{control}} - \text{OD}_{\text{blank}})}{\times 100\%}$$

where $\text{OD}_{\text{experimental}}$ represents optical density of cells cultured with wound dressings; and OD_{blank} represents absorbance of the well plate, and $\text{OD}_{\text{control}}$ represents absorbance of the cells without any treatment.

2.10.2. The Live/Dead Fluorescence Assay. The 3T3 cells were seeded in glass culture dishes overnight. Then, the extract liquid of HA/SF/Alg, Rb-BG-AIEgens/H A/SF/Alg, and HA-AMP/SF/Alg/Rb-BG-AIEgens were incubated with the cells for 24 h. The 3T3 cells were washed with PBS three times and stained with the Clacein/PI live/dead fluorescence dye following the instruction. The cells were further observed

with confocal laser scanning microscopy (CLSM, Leica, Germany) to evaluate the biocompatibility.

2.10.3. Cell Migration. The in vitro cell migration assay was performed to estimate the influence of HA/SF/Alg, Rb-BG-AIEgens/H A/SF/Alg, and HA-AMP/SF/Alg/Rb-BG-AIEgens on 3T3 cells. Cells were seeded at density of 2×10^5 cells/well in 12 well plates and incubated overnight. Then, a straight line was made by a pipet tip. Cells were washed twice with PBS solution and added the extract liquid containing medicine. After specific incubation periods, cells were visualized via microscope (Olympus IX71, Japan).

2.11. Establishment of Infected Wound and Evaluation of Therapeutic Effect.

2.11.1. Wound Healing In Vivo.

To investigate the potential efficacy of composite wound dressings for skin wound healing, female New Zealand rabbits (2.5 kg) of free breeding were first shaved and anesthetized with 0.5% sodium pentobarbital. After sterilizing the skin with 75% alcohol, a round full-thickness cutaneous incision 20 mm in diameter was made on the back of each rabbit. 100 μL 1×10^8 CFU/mL mixed with bacterial solution of *E. coli* and *S. aureus* was injected into to each wound to establish the infected wound model. Defects were covered with composite hydrogel after 24 h. Each rabbit was numbered and randomly divided into 4 groups: medical gauze (blank control group), Rb-BG-AIEgens, Rb-BG-AIEgens/H A/SF/Alg, and HA-AMP/SF/Alg/Rb-BG-AIEgens. The wound surface was

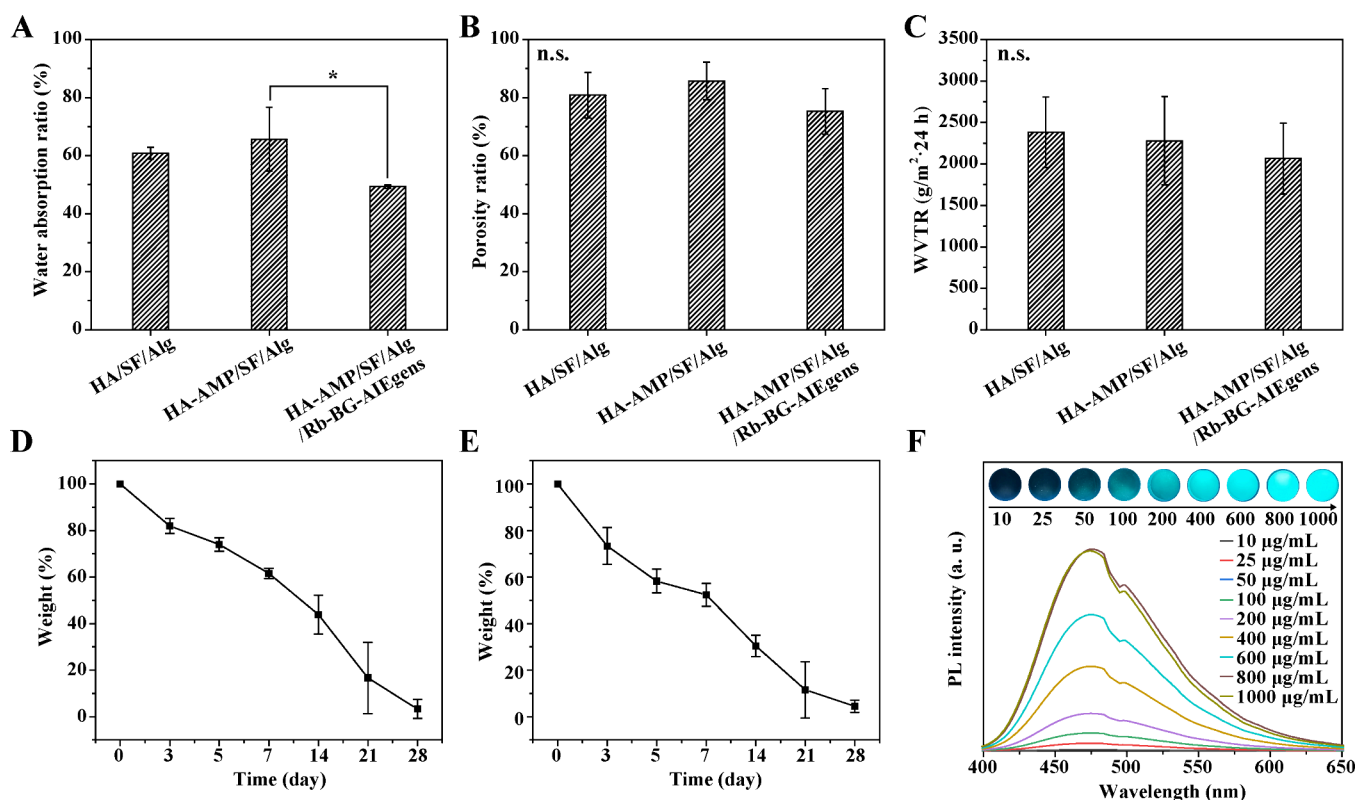


Figure 2. Physical properties of HA-AMP/SF/Alg/Rb-BG-AIEgens wound dressing. (A) Water absorption, (B) porosity ratio, and (C) water vapor transmission rate of different dressings; (D) the weight change curve of wound dressing degraded in PBS and (E) enzyme environment; and (F) fluorescence intensity of Rb-BG-AIEgens at different mass concentrations.

closed with different materials according to the above groups, and then covered with 3 M Tegaderm waterproof tape for fixation. Each rabbit was observed and photographed at day 1, 5, 10, 18, and 24 after surgery to observe the chronic wound healing changes. The wound area was determined with ImageJ software, and the skin wound healing rate (%) was calculated according to the following formula:

$$\text{skin wound healing rate (\%)} = \frac{(\text{initial wound area} - \text{real wound area})}{\text{initial wound area}} \times 100\%$$

2.11.2. Histology and Immunohistochemistry. The morphology of wound skin was observed by histopathological sections. On the 10th day, the skin tissues were excised from the back of rabbits and fixed with 4% paraformaldehyde solution. The embedded skin tissues and other major organs were sectioned into slices for staining. The sections were stained with hematoxylin-eosin (H&E) and Masson's trichrome staining (Masson) staining. Then, stained samples were observed on an optical microscope system (Olympus IX-71, Japan).

2.12. Statistical Analysis. All data were recorded as mean \pm standard deviation (SD) with statistical analysis by GraphPad Prism 9.5 software. Comparisons between multiple groups were analyzed using one-way analysis of variance (ANOVA) (* $p < 0.05$, ** $p < 0.01$, and *** $p < 0.001$).

3. RESULTS

3.1. Synthesis and Characterizations of HA-AMP/SF/Alg/Rb-BG-AIEgens Composite Wound Dressing. First, we designed a chemically grafted HA-AMP to enhance the antibacterial and biocompatibility for dressing (Figure 1B).

FTIR was further performed on the HA-AMP to analyze the chemical formation. As shown in Figure 1A, the characteristic stretching vibration of $-\text{NH}$ at absorption band of 1643 cm^{-1} can be observed in the FT-IR spectrum of HA-AMP. The peak at 1620 cm^{-1} corresponded to the $-\text{NH}_2$ peak in HA, which attributed to condensation of the carboxyl group on activated HA with the amino group on AMP. In addition, a characteristic absorption peak at approximately 1380 cm^{-1} can be observed, further confirming the successful synthesis of HA-AMP. ^1H nuclear magnetic resonance (^1H NMR) was used for confirming whether HA and AMP were successfully grafted. HA-AMP was a copolymer which synthesized based on EDC/NHS coupling technology. Briefly, EDC/NHS functionalized the carboxyl group on HA as the cross-linking agent, and then the carboxyl group binding with the amino group on AMP through condensation reaction, thereby the AMP was grafted onto the main chain of hyaluronic acid by an amide bond to form HA-AMP. The ^1H NMR pattern of HA-AMP shown the ester group peak at 2.8 ppm, proving the successful synthesis of HA-AMP (Figure 1B).

As shown in Figure 1C, bioactive mesoporous silicon composed of Rb-BG presented a uniform sheet shape. The addition of AIEgens had no significant changes for mesoporous silicon materials. The SEM images show the morphology of the prepared wound dressing. Herein, the network of the wound dressing formed involving both SF, Alg, and HA chains. SF, Alg, and HA acted as the substrate of hydrogel due to their excellent gelation properties, biodegradability, and cytocompatibility.³⁷ As shown in Figure 1D, all composite wound dressings had a clear pore structure in surface and the cross sections. However, the pore structures of different HA/SF/Alg

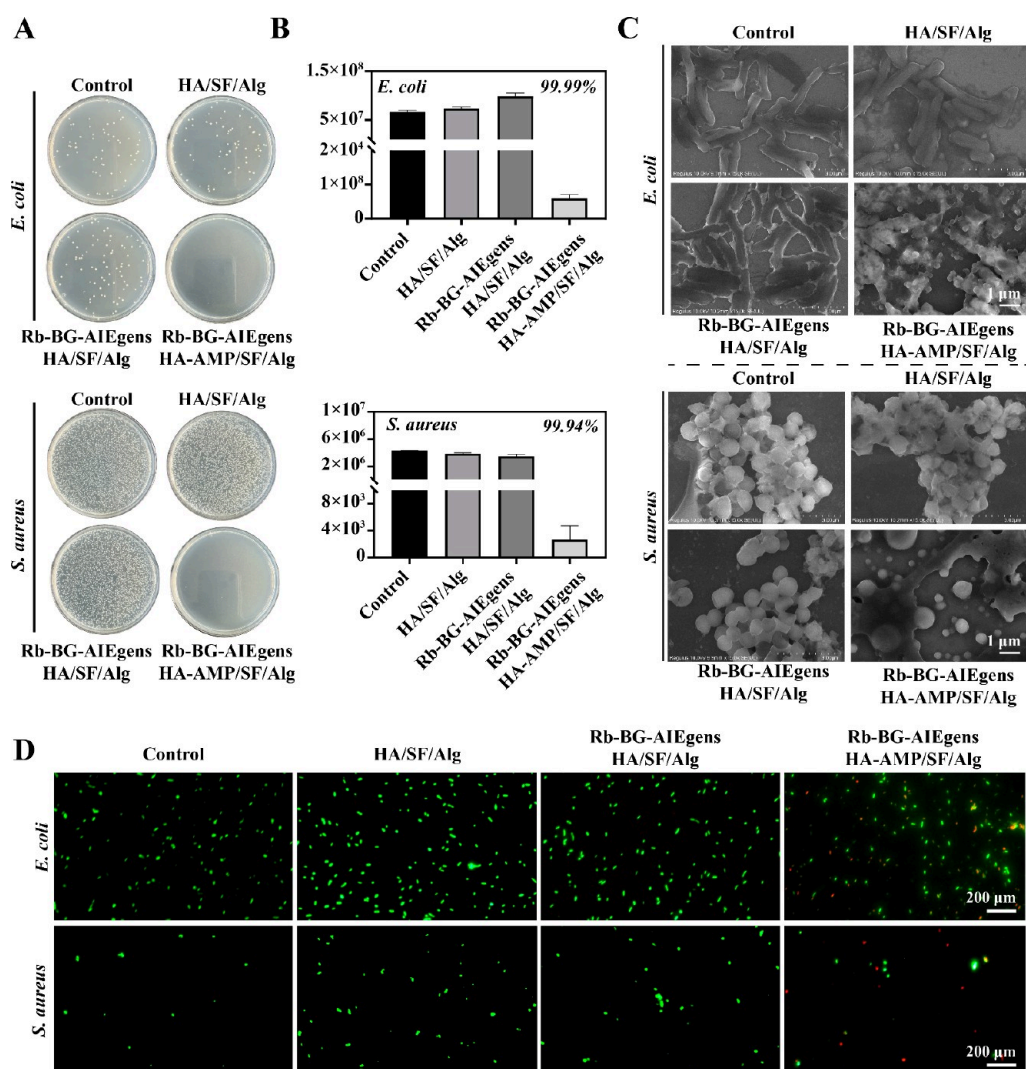


Figure 3. In vitro antibacterial activity. (A) Number of colonies on agar plates after cocultivation with antibacterial dressings; (B) colony statistics and antimicrobial rates; (C) SEM images of *E. coli* and *S. aureus*; and (D) live (green) and dead (red) fluorescence staining images of *E. coli* and *S. aureus*.

composite wound dressings show some differences. When Rb-BG-AIEgens was added, the pore size decreased in HA-AMP/SF/Alg/Rb-BG-AIEgens. There was a possibility that bioactive mesoporous materials filled part of the gaps, thus making the wound dressing network structure denser. The loose and porous sponge structure facilitates faster moisture absorption and water locking, helping to maintain hydration at the wound site. Therefore, the HA-AMP/SF/Alg/Rb-BG-AIEgens composite wound dressings with microporous structure could be beneficial to the absorption of wound exudates and promote wound recovery when they served as scaffolds for wound regeneration.

3.2. Mechanical Behavior of HA-AMP/SF/Alg/Rb-BG-AIEgens. Absorbing a large amount of wound exudates is beneficial to wound healing. To evaluate the hydro absorption capacity of HA-AMP/SF/Alg/Rb-BG-AIEgens, we evaluated the weight difference of the samples before and after moisture absorption via extrusion and immersion. The experimental results presented that all groups could achieve more than 50% water absorption rate (Figure 2A). The group of HA-AMP/SF/Alg/Rb-BG-AIEgens had a lower amount and rate of water absorption when compared with Alg/SF/HA-AMP. This

difference may be due to the size effects of the nanopore structure and the tight pore.³⁸ We speculate that the rate of water absorption of HA-AMP/SF/Alg/Rb-BG-AIEgens and Alg/SF/HA-AMP are mainly related to the capillary force caused by their porous structure and dimensions. We further demonstrated the porosity of composite sponge films as shown in Figure 2B. The results have shown that the porosity of HA-AMP/SF/Alg/Rb-BG-AIEgens was slightly lower than that of Alg/SF/HA-AMP, revealing that the addition of Rb-BG-AIEgens increased cross-linking density. The increase of cross-linking points made the internal pores of the hydrogel dressing smaller and the internal structure of the hydrogel closer, which eventually contributed to the gradual reduction of the pores of the sponge sample after freeze-dried. Also, the dense porous structure and more pore numbers of HA-AMP/SF/Alg/Rb-BG-AIEgens could improve the water locking capacity and maintain the osmotic balance of the wound.

As shown in Figure 2C, Alg/SF/HA had the highest WVTR, reached $2383.59 \pm 426.92\%$. With the addition of AMP, the WVTR of Alg/SF/HA-AMP decreased slightly ($2278.93 \pm 532.56\%$), which retarded the water loss rate of the hydrogel wound dressing. The WVTR of HA-AMP/SF/Alg/Rb-BG-

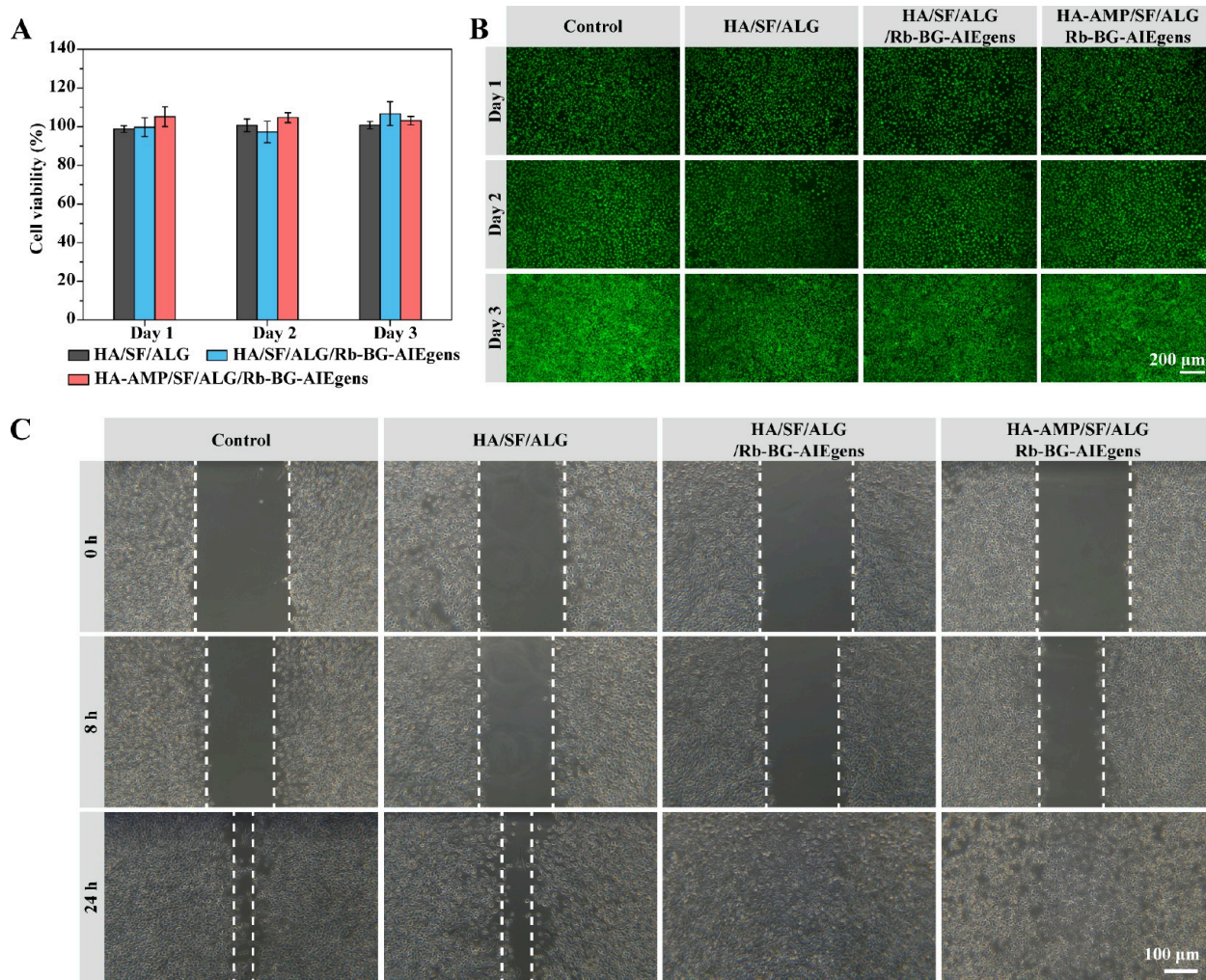


Figure 4. Cytotoxicity and migration of 3T3 cells. (A) The cell viability of 3T3 cells after coculture with the dressing extract via CCK-8 method. (B) Live and dead cell staining. (C) Migration images of 3T3 cells treated with a dressing extract. Scale bar: 100 μm .

AIEgens achieved $2067.31 \pm 428.64\%$ ranged from 1500 to 2500 $\text{g}/\text{m}^2/24 \text{ h}$ at 37 $^{\circ}\text{C}$, indicating that the composite hydrogel film was effective in reducing water evaporation and keeping the wound moist.

The appropriate degradation rate was helpful for wound recovery. We evaluated the degradation of the dressing by in vitro PBS solution and PBS containing lysozyme. The degradation progression over time was presented by weighting the degree of HA-AMP/SF/Alg/Rb-BG-AIEgens loss immersed in PBS solution (Figure 2D,E). Both curves show a gradual decrease in degradation rate with time. However, the dressing showed a faster degradation rate in PBS containing lysozyme compared with PBS solution only. Therefore, we speculated that scaffold degradation was limited by the media environment, which affected dressing dissolution and hydrolysis. It was further demonstrated that the HA-AMP/SF/Alg/Rb-BG-AIEgens dressing was an enzyme responsive material, which could accelerate hydrolysis in the presence of enzymes and promote skin regeneration.

Specific fluorescent material of AIEgens was nonbloomed in the state of molecular dispersion and emitted strong light only in the state of aggregation. Therefore, we used fluorescence spectroscopy to determine whether Rb-BG-AIEgens were successfully grafted, the intensity of Rb-BG-AIEgens fluorescence gradually increased with increasing concentration of

AIEgens (Figure 2F). In addition, a characteristic absorption peak at approximately 475 nm can be observed in the UV-vis spectrum. This might be due to the gradual aggregation of hydrophobic units with enhanced AIEgens concentration, which resulted in an increased intensity of the emission peak at 475 nm. The mechanical properties of the HA/SF/Alg dressings are displayed in Table S1 of the Supporting Information. The Young's modulus of the dressings reaches over 20 MPa, while the tensile strength of the Rb-BG-AIEgens/HA-AMP/SF/Alg dressings is measured at $0.23 \pm 0.05 \text{ MPa}$. The elongation at break for all three types of dressings is less than 25%. The mechanical performance of the dressings we have prepared is sufficiently robust for use as wound dressings in clinical.

3.3. Antibacterial Experiments In Vitro. Antibacterial ability is important for wound dressing. The HA-AMP/SF/Alg/Rb-BG-AIEgens group shows a significant kill effect of *E. coli* and *S. aureus* compared with the other groups (Figure 3A). The inhibitory effect of HA-AMP/SF/Alg/Rb-BG-AIEgens on *E. coli* and *S. aureus* could reach more than 99%, indicating the best antibacterial activity (Figure 3B). We further assessed the killing ability of the wound dressings by bacterial SEM images and live/death staining. As shown in Figure 3C&D, the morphology of bacteria in the group without any treatment was smooth and intact, and a large number of viable cells

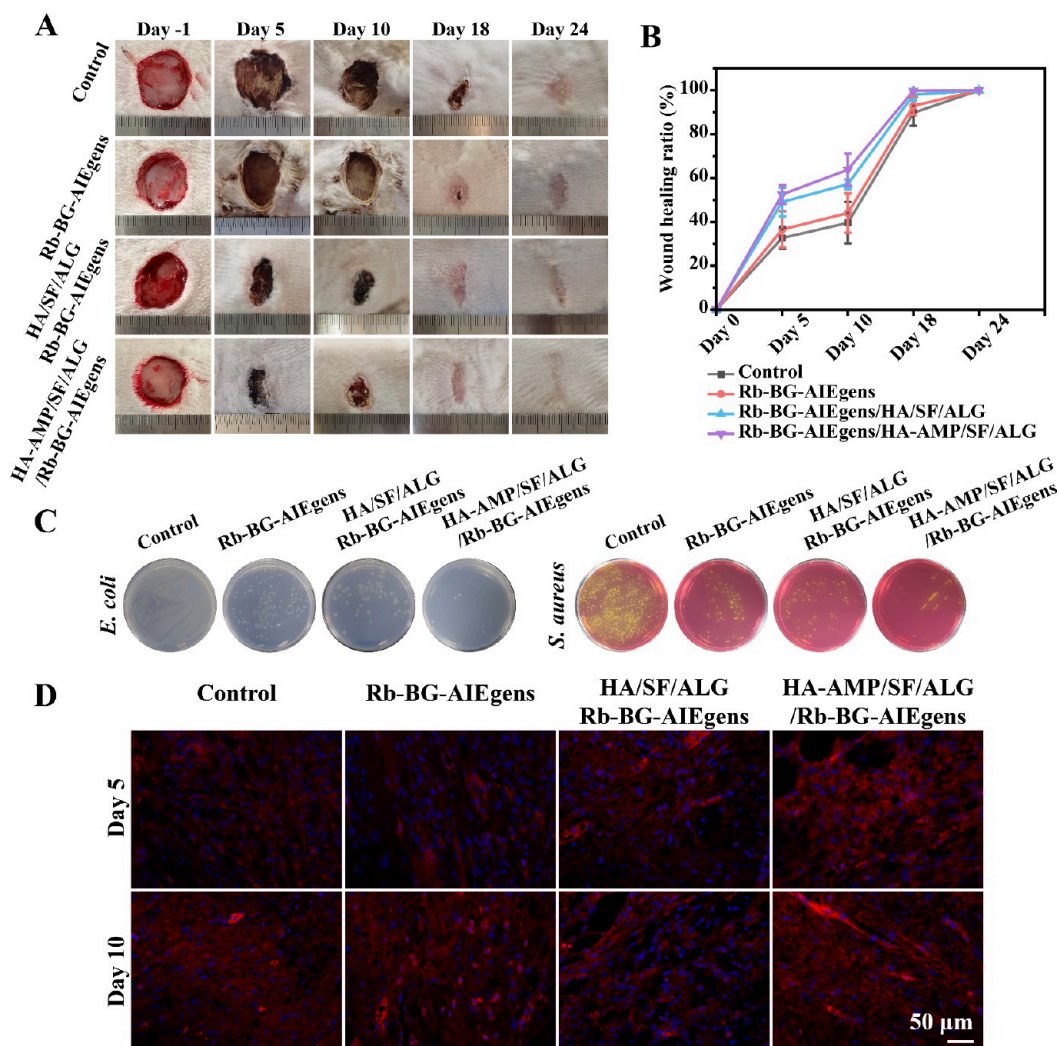


Figure 5. (A) Wound images of skin at different time points; (B) healing curve of wound area; (C) image of agar plates of colonies of *E. coli* and *S. aureus* from a skin sample on selective medium; and (D) immunofluorescence staining of MPO; scale bar: 50 μm .

(green) were found under fluorescent staining. However, wound dressings undergoing antimicrobial peptides obviously killed the bacteria. The dead bacteria labeled with red fluorescence could be seen in fluorescence confocal images, and the bacterial morphology was incomplete, wrinkled, shrunken, or ruptured in SEM images.

We further determined the ability of antimicrobial dressing to inhibit bacterial population growth in three sewage samples (Figure S1). The results of resistance to bacterial erosion suggested that the HA-AMP/SF/Alg/Rb-BG-AIEgens could significantly reduce the number of bacteria and lethally kill them.

3.4. Cytotoxicity In Vitro. To determine the cytotoxicity of HA-AMP/SF/Alg/Rb-BG-AIEgens, a quantitative evaluation of 3T3 cells was carried out by CCK-8 method. After 72 h of culture, all dressings cocultured groups shown low cytotoxicity against 3T3 cells (Figure 4A). The cell survival rates of HA-AMP/SF/Alg/Rb-BG-AIEgens were above 100% after coculture, indicating the excellent biocompatibility.

To further verify the cytocompatibility of HA-AMP/SF/Alg/Rb-BG-AIEgens composite dressing, we carried out live/dead staining by Calcein/PI, which was shown in Figure 4B. The 3T3 cells cultured with the wound dressing had good vitality after 24 h of culture, and there was nearly no difference

compared with the control group. By increasing the coculture time to 48 and 72 h, the density of living 3T3 cells (green fluorescence) had a further increase, and scarcely any dead cells (red fluorescence) could be found, indicating that the wound dressing would not cause cytotoxicity to the 3T3 cells.

We further estimated the effect of HA-AMP/SF/Alg/Rb-BG-AIEgens composite dressing on cell migration behaviors via cell scratch test. Fibroblasts are one of the main cells in wound healing, thus 3T3 cells were used for scratch assays. It could be seen from Figure 4C that the 3T3 cells treated with different composite dressings had a facilitated tendency of growing to the middle gap. The cell migration behavior of HA-AMP/SF/Alg/Rb-BG-AIEgens slightly surpassed that of the control group. The reason for this phenomenon might be that the dressings we prepared promoted secretion of growth factor collagen fibers from 3T3, which further accelerated wound healing.³⁹

3.5. In Vivo Infected Wound Healing. The bacterial inhibition in vivo and the wound healing efficacy of HA-AMP/SF/Alg/Rb-BG-AIEgens was evaluated by the infectious skin defect model. The progression of the whole infected wound healing in vivo study was illustrated in Figure 5. The full-thickness rabbits were divided into four groups randomly: infection group (control), Rb-BG-AIEgens group, HA/SF/

Alg/Rb-BG-AIEgens group, and HA-AMP/SF/Alg/Rb-BG-AIEgens group. As shown in Figure 5A, the HA-AMP/SF/Alg/Rb-BG-AIEgens wound dressing group showed an obvious wound healing ratio compared to the others. On the 10th day, the HA-AMP/SF/Alg/Rb-BG-AIEgens treated wounds almost completely healed when obvious skin defects were still visible in the control groups. The quantitative data of wound healing indicate that the wound healing rate in the HA-AMP/SF/Alg/Rb-BG-AIEgens group had reached $61.5 \pm 2.2\%$ on the 10th day, the other groups needed 15 days to reach this healing rate (Figure 5B). On the 18th day, the HA-AMP/SF/Alg/Rb-BG-AIEgens group was almost healed and covered by new epithelial tissue.

The infection also influenced the wound healing, which is significantly related to the wound microenvironment. The antibacterial and bacterial capture abilities of dressings were evaluated with *E. coli* and *S. aureus*. The composite Rb-BG-AIEgens-AMP/HA/SF/Alg dressings show significant inhibition of *S. aureus* and *E. coli* growth compared with the control (Figure 5C). The HA-AMP/SF/Alg/Rb-BG-AIEgens group could effectively prevent infection, and there was no excessive exudate around the wound, which is mainly due to bacterial capture and damage to bacteria by AMP. The chemical grafting of HA-AMP through amidation could effectively improve the antibacterial and biocompatibility of composite dressings.⁴⁰

Myeloperoxidase (MPO) is the most bactericidal oxidant produced by neutrophils.⁴¹ It can serve as the antibacterial marker in tissue. Figure 5D showed that the expression of MPO was significantly increased in the HA-AMP/SF/Alg/Rb-BG-AIEgens-treated group, demonstrating the potent ability to kill harmful bacteria. After 10 days of treatment, HA-AMP/SF/Alg/Rb-BG-AIEgens wound dressing treated group still exhibited the highest MPO immunofluorescence intensity and displayed excellent antibacterial function compared to the HA/SF/Alg/Rb-BG-AIEgens group.

3.6. Histological Analyze. Giemsa staining of the control group and the Rb-BG-AIEgens group showed that a large number of bacteria existed in the wounds after treating for 5 days. The HA/SF/Alg/Rb-BG-AIEgens group also had bacteria, but the number was small. When the wounds were treated for 10 days, the bacteria in the HA-AMP/SF/Alg/Rb-BG-AIEgens groups were less (Figure 6A). H&E and Masson's trichrome staining verified that HA-AMP/SF/Alg/Rb-BG-AIEgens had a more obvious effect on promoting wound healing. On the 10th day, more fibroblasts were observed and inflammatory infiltration was also absent. Additionally, more new blood vessels and new skin appearing in the HA-AMP/SF/Alg/Rb-BG-AIEgens composite hydrogel film group, indicating better tissue regeneration at the wound sites (Figure 6B). Collagen plays an essential role in wound healing. We can observe the obvious collagen deposition in the HA-AMP/SF/Alg/Rb-BG-AIEgens group by Masson's staining (Figure 6C), implying a better ability of the tissue rearrangement for wound healing. We quantitatively analyzed collagen deposition using Masson's trichrome staining. During the wound healing process, collagen initially accumulates to fill the damaged area. As the treatment period progresses, collagen undergoes rearrangement and absorption to prevent excessive deposition that could lead to scarring. Quantitative analyses of Masson's trichrome staining at 10 and 18 days post-treatment were conducted. After 18 days of treatment, the dressing group exhibited a significantly greater amount of collagen deposition compared to the control group (Figure S2). By day 24 of

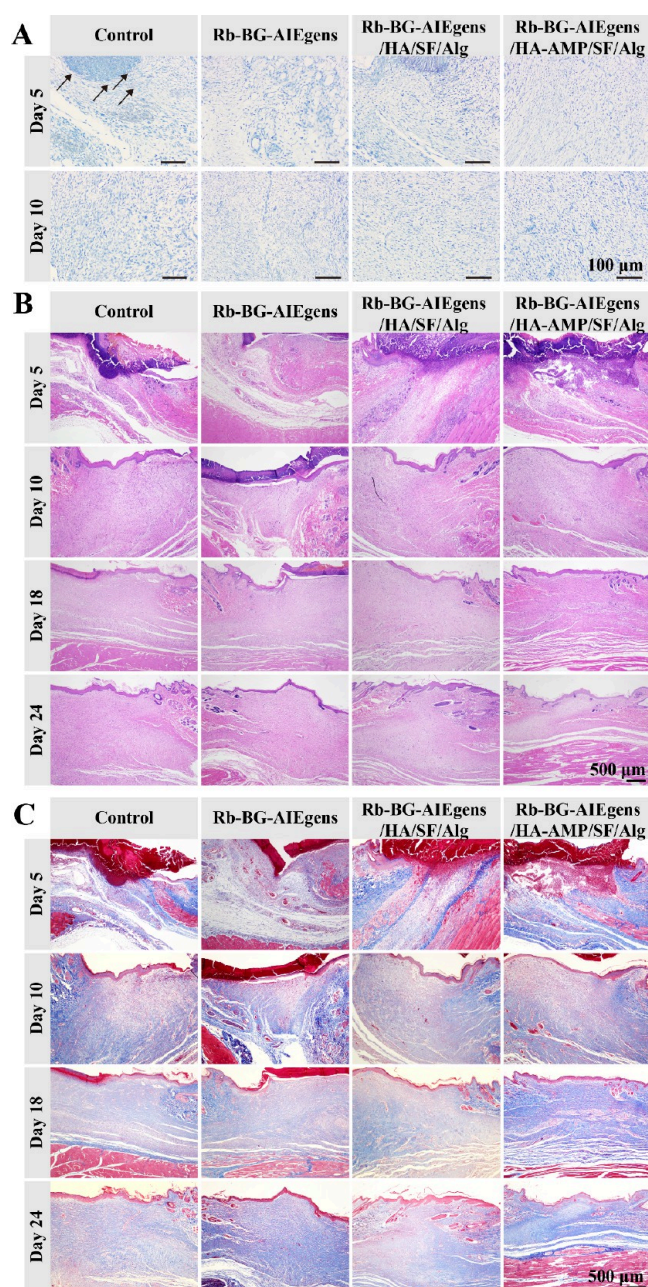


Figure 6. Histological evaluation of skin healing quality. (A) Giemsa staining of skin on the 5th and 10th day after treating; (B) H&E and (C) Masson staining of wound tissue at 5th, 10th, 18th, and 24th day after treatment.

treatment, collagen absorption in the Alg group was observed, with the regenerated skin tissue gradually returning to its normal morphology.

The wound recovery process can be affected by the inflammatory response, related inflammatory markers, including tumor necrosis factor (TNF- α), interleukin-4 (IL-4), interferon- γ (IFN- γ), and tumor growth factor- β 1 (TGF- β 1) were selected to evaluate the ability of resistance to infection of different composite wound dressings. The TNF- α in the Rb-BG-AIEgens group was higher than the HA-AMP/SF/Alg/Rb-BG-AIEgens group after 10 days of treatment (Figure 7A). As shown in Figure 7B, the positive area of IFN- γ significantly reduced, implying that HA-AMP/SF/Alg/Rb-BG-AIEgens can inhibit the production of inflammation. The superior perform-

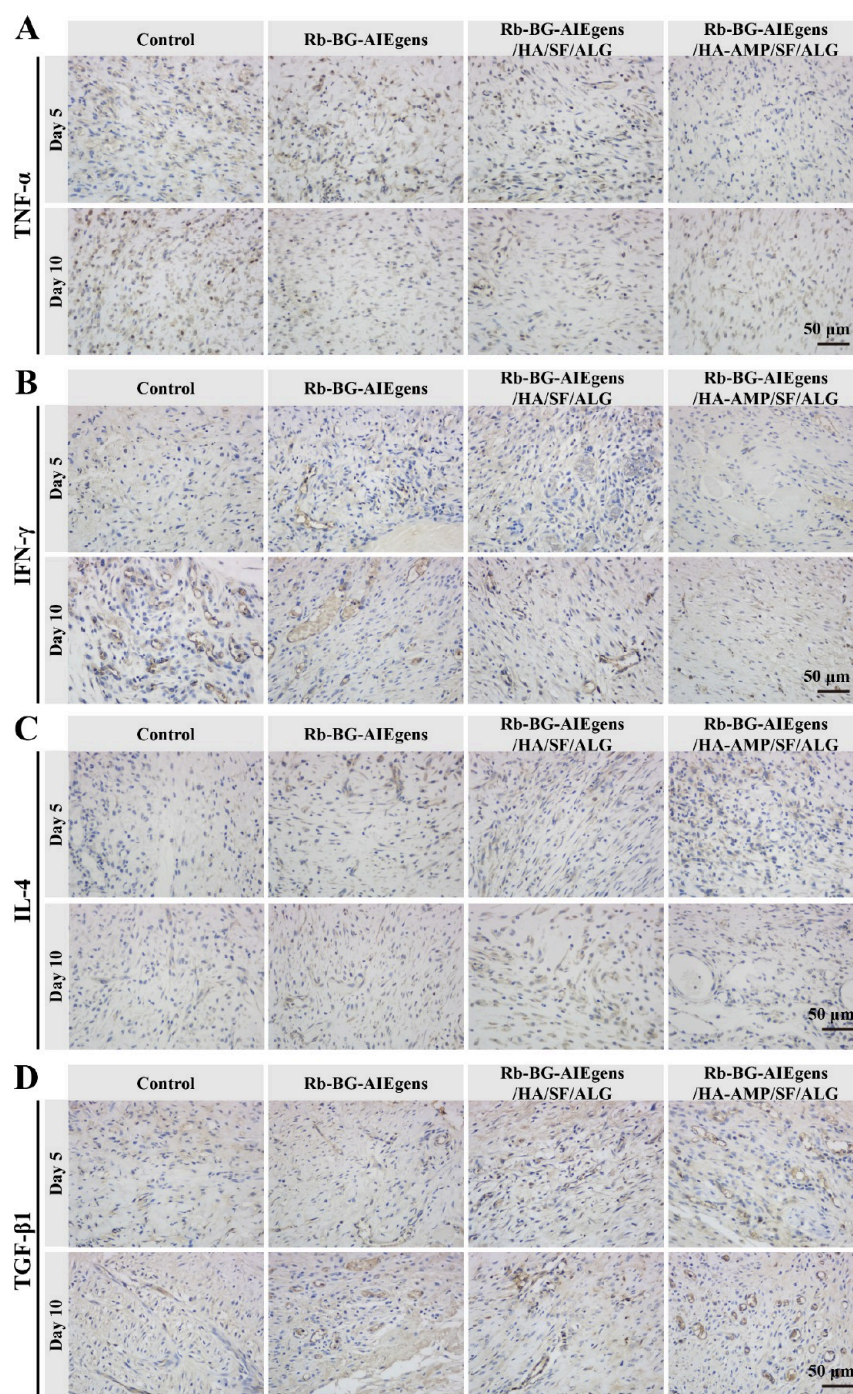


Figure 7. Histological evaluation of skin healing quality. Immunohistochemical staining of inflammatory factors (A) TNF- α , (B) IL-4, (C) IFN- γ , and (D) TGF- β 1; scale bar = 50 μ m.

ance of the preparation was also demonstrated by the decreased expression of related anti-inflammatory factors, such as IL-4 (Figure 7C) and TGF- β 1 (Figure 7D, Figure S3).

3.8. H&E Staining Showed No Toxicity to Major Organs. As shown in Figure 8, H&E staining confirmed favorable biological safety in vivo of HA-AMP/SF/Alg/Rb-BG-AIEgens. After 24 days of treatment with different dressings, no apparent histological abnormality was detected in the main organs including heart, liver, spleen, lung, and kidney, indicating good biocompatibility in all groups. In conclusion, these results collectively demonstrated that HA-AMP/SF/Alg/Rb-BG-AIEgens was promising as an effective

wound microenvironment management dressing for further practical application.

4. DISCUSSION

The mechanism of bacterial infection-related wound healing encompasses various factors, such as heightened inflammatory responses, cellular damage and apoptosis, degradation of the extracellular matrix, impaired angiogenesis, immune suppression,^{42,43} and biofilm formation. These interrelated mechanisms collectively impede wound healing, prolonging the healing process and heightening the risk of complications. To achieve the goal of promoting wound healing, Yang et al.⁴⁴

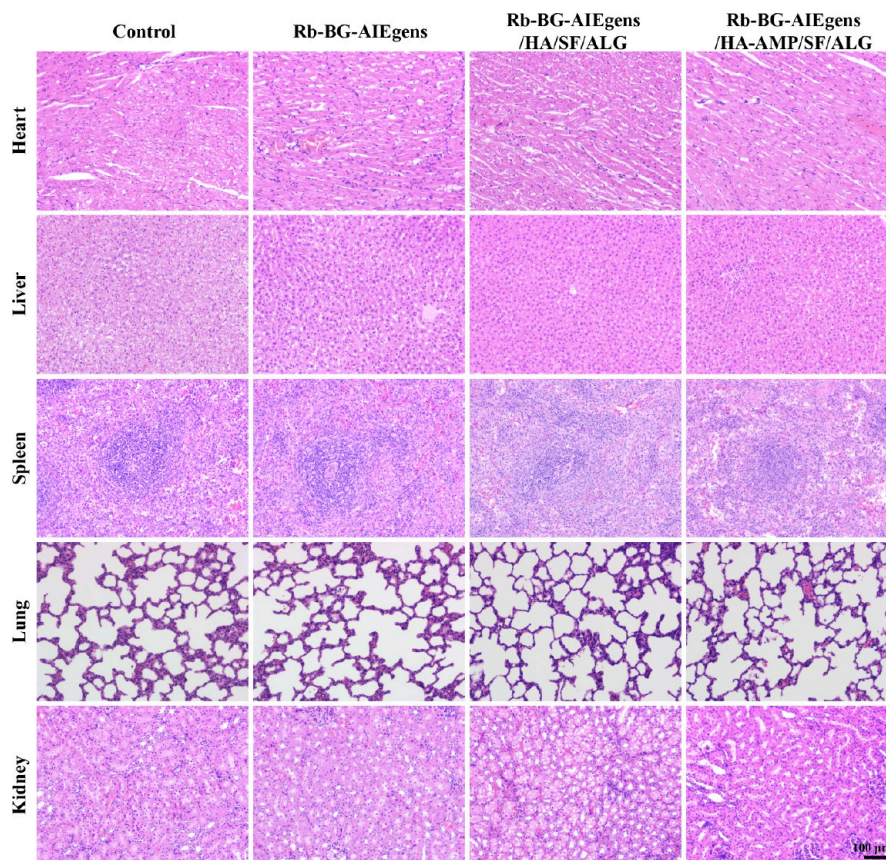


Figure 8. H&E staining of major organs after treating for 24 days; scale bar = 100 μm .

design a three-dimensional tricopolymer scaffold to investigate skin reconstruction by right of ternary blends of the three biomacromolecules, SF, HA, and Alg. Their research findings illustrate that the SF/HA/SA composite scaffold offers an advantageous milieu for wound healing and exhibits an efficient degradation rate conducive to dermal repair. This facilitates enhanced collagen deposition and contributes to substantial skin reconstruction. The AMP hydrogel, as designed and evaluated by Saba et al.,⁴⁵ demonstrates outstanding performance, rendering it an optimal wound dressing with preventive attributes against infection and facilitative effects on wound healing. MP-hydrogels have an ability to kill a broad range of bacterial species including antibiotic-resistant strains, representing a preventive wound dressing that can decrease microbial bioburden and risk of infection in the wound. Kang et al.⁴⁶ reported that AIEgens demonstrate near-infrared (NIR) emission properties, obviating the need for supplementary targeting moieties, allowing for selective staining of Gram-positive bacteria, coupled with remarkably high efficiency in ROS generation. This facilitates swift and thorough inactivation of Gram-positive bacteria in both in vitro and in vivo settings.

Inspired by the aforementioned studies, in this research, antimicrobial peptide (AMP) was conjugated with hyaluronic acid (HA) via an amide reaction to form HA-AMP, serving as an antibacterial peptide chain for bactericidal activity. Subsequently, HA-AMP was grafted onto functionalized SF/Alg sponges, and a composite dressing, HA-AMP/SF/Alg/Rb-BG-AIEgens, was designed utilizing a mesoporous bioactive glass framework (Rb-BG-AIEgens) as a cross-linker, facilitating dual effects of bacterial monitoring and sterilization. Moreover,

the composite dressing, HA-AMP/SF/Alg/Rb-BG-AIEgens, demonstrates synergistic antibacterial and immunomodulatory properties, capable of eradicating bacteria within the wound bed, mitigating inflammation, ensuring anti-infection effects, and promoting wound healing.

5. CONCLUSIONS

In this work, the antibacterial AMP were successfully grafted into the biocompatible HA-AMP/SF/Alg/Rb-BG-AIEgens composite dressing for biofluid management and wound disinfection. The HA-AMP/SF/Alg/Rb-BG-AIEgens showed good mechanical properties, including porous structure, hydrophilicity, and high water permeability, which are favorable for cell adhesion and rapid liquid absorption of wound exudate. Additionally, the results shown that HA-AMP/SF/Alg/Rb-BG-AIEgens composite dressing had excellent biocompatibility. In vivo experiments proved that the HA-AMP/SF/Alg/Rb-BG-AIEgens composite dressing could not only accelerate the wound healing process but also promote the deposition of collagen and re-epithelialization, which were confirmed by H&E and Masson histological staining. Histological analysis showed that HA-AMP/SF/Alg/Rb-BG-AIEgens could effectively promote the expression of related proliferative proteins, and further promote tissue regeneration and wound healing. After 10 days, it was observed that only the HA-AMP/SF/Alg/Rb-BG-AIEgens group exhibited a wound healing rate of over 60%, with concomitant inhibition of inflammatory factor production. In addition, the prepared composite dressing had bacteria adaptively and actively attacked *E. coli* and *S. aureus*, as well as reshaped the microenvironment of wound. This study developed a HA-

AMP/SF/Alg/Rb-BG-AIEgens as-fabricated wound dressing and demonstrated favorable biological capabilities in promoting antibacterial wound healing.

■ ASSOCIATED CONTENT

SI Supporting Information

The Supporting Information is available free of charge at <https://pubs.acs.org/doi/10.1021/acsomega.4c00649>.

Antibacterial erosion plate images, dressing tensile properties, collagen deposition, and quantitative statistical charts of inflammatory factors (PDF)

■ AUTHOR INFORMATION

Corresponding Authors

Biao Cheng – Department of Burns and Plastic Surgery, General Hospital of Southern Theater Command, PLA, Guangzhou 510010, P. R. China; Email: chengbiaocheng@163.com

Yi Chen – Department of Cadre Ward, General Hospital of Southern Theater Command, PLA, Guangzhou 510010, P. R. China; orcid.org/0009-0009-2594-7608; Email: Yihan_816@163.com

Authors

Yize Lin – Graduate School, Guangzhou University of Traditional Chinese Medicine, Guangzhou 510006, P. R. China

Yan Tan – Department of Cadre Ward, General Hospital of Southern Theater Command, PLA, Guangzhou 510010, P. R. China

Rong Deng – Department of Health Medicine, General Hospital of Southern Theater Command, PLA, Guangzhou 510010, P. R. China

Li Gong – Department of Cadre Ward, General Hospital of Southern Theater Command, PLA, Guangzhou 510010, P. R. China

Xiaoshan Feng – Department of Cadre Ward, General Hospital of Southern Theater Command, PLA, Guangzhou 510010, P. R. China

Zhongqi Cai – Department of Cadre Ward, General Hospital of Southern Theater Command, PLA, Guangzhou 510010, P. R. China

Yanxian He – Department of Cadre Ward, General Hospital of Southern Theater Command, PLA, Guangzhou 510010, P. R. China

Longbao Feng – Key Laboratory of Biomaterials of Guangdong Higher Education Institutes, Guangdong Provincial Engineering and Technological Research Centre for Drug Carrier Development, Department of Biomedical Engineering, Jinan University, Guangzhou 510632, P. R. China

Complete contact information is available at: <https://pubs.acs.org/doi/10.1021/acsomega.4c00649>

Author Contributions

[#]These authors contributed equally to this work.

Notes

The authors declare no competing financial interest.

■ ACKNOWLEDGMENTS

The authors would like to express their sincere gratitude to the General Hospital of Southern Theater Command, PLA and

Jinan University for their support and resources, which provided valuable experimental conditions, cooperation, and guidance for the completion of this study.

■ REFERENCES

- (1) Aitcheson, S. M.; Frentiu, F. D.; Hurn, S. E.; Edwards, K.; Murray, R. Z. Skin Wound Healing: Normal Macrophage Function and Macrophage Dysfunction in Diabetic Wounds, *Molecules*. *Mol.* **2021**, *26* (16), 4917.
- (2) Powers, J. G.; Higham, C.; Broussard, K.; Phillips, T. J. Wound healing and treating wounds: Chronic wound care and management. *J. Am. Acad. Dermatol.* **2016**, *74* (4), 607–25.
- (3) Rippon, M. G.; Rogers, A. A.; Ousey, K. Antimicrobial stewardship strategies in wound care: evidence to support the use of dialkylcarbonyl chloride (DACC)-coated wound dressings. *Journal of wound care* **2021**, *30* (4), 284–296.
- (4) Dong, R.; Guo, B. Smart wound dressings for wound healing. *Nano Today* **2021**, *41*, 101290.
- (5) Farahani, M.; Shafiee, A. Wound Healing: From Passive to Smart Dressings. *Adv. Healthcare Mater.* **2021**, *10* (16), e2100477.
- (6) Kalantari, K.; Mostafavi, E.; Afifi, A. M.; Izadiyan, Z.; Jahangirian, H.; Rafiee-Moghaddam, R.; Webster, T. J. Wound dressings functionalized with silver nanoparticles: promises and pitfalls. *Nanoscale* **2020**, *12* (4), 2268–2291.
- (7) Huang, Q.; Wu, T.; Wang, L.; Zhu, J.; Guo, Y.; Yu, X.; Fan, L.; Xin, J. H.; Yu, H. A multifunctional 3D dressing unit based on the core-shell hydrogel microfiber for diabetic foot wound healing. *Biomaterials science* **2022**, *10* (10), 2568–2576.
- (8) Wang, Z.; Zhang, Y.; Yin, Y.; Liu, J.; Li, P.; Zhao, Y.; Bai, D.; Zhao, H.; Han, X.; Chen, Q. High-Strength and Injectable Supramolecular Hydrogel Self-Assembled by Monomeric Nucleoside for Tooth-Extraction Wound Healing, Advanced materials (Deerfield Beach, FL). *Adv. Mater.* **2022**, *34* (13), e2108300.
- (9) Boateng, J.; Catanzano, O. Advanced Therapeutic Dressings for Effective Wound Healing—A Review. *Journal of pharmaceutical sciences* **2015**, *104* (11), 3653–3680.
- (10) Ramanathan, G.; Seleenmary Sobhanadhas, L. S.; Sekar Jayakumar, G. F.; Devi, V.; Sivagnanam, U. T.; Fardim, P. Fabrication of Biohybrid Cellulose Acetate-Collagen Bilayer Matrices as Nano-fibrous Spongy Dressing Material for Wound-Healing Application. *Biomacromolecules* **2020**, *21* (6), 2512–2524.
- (11) Vega, S. L.; Kwon, M. Y.; Burdick, J. A. Recent advances in hydrogels for cartilage tissue engineering. *European cells & materials* **2017**, *33*, 59–75.
- (12) Graça, M. F. P.; Miguel, S. P.; Cabral, C. S. D.; Correia, I. J. Hyaluronic acid-Based wound dressings: A review. *Carbohydr. Polym.* **2020**, *241*, 116364.
- (13) Litwiniuk, M.; Krejner, A.; Speyrer, M. S.; Gauto, A. R.; Grzela, T. Hyaluronic Acid in Inflammation and Tissue Regeneration. *Wounds* **2016**, *28* (3), 78–88.
- (14) Yin, C.; Qi, X.; Wu, J.; Guo, C.; Wu, X. Therapeutic contact lenses fabricated by hyaluronic acid and silver incorporated bovine serum albumin porous films for the treatment of alkali-burned corneal wound. *Int. J. Biol. Macromol.* **2021**, *184*, 713–720.
- (15) Zhao, Y.; Li, Y.; Peng, X.; Yu, X.; Cheng, C.; Yu, X. Feasibility study of oxidized hyaluronic acid cross-linking acellular bovine pericardium with potential application for abdominal wall repair. *Int. J. Biol. Macromol.* **2021**, *184*, 831–842.
- (16) Kundu, B.; Rajkhowa, R.; Kundu, S. C.; Wang, X. Silk fibroin biomaterials for tissue regenerations. *Adv. Drug Deliv. Rev.* **2013**, *65* (4), 457–70.
- (17) Lujerdecian, C.; Baci, G. M.; Cucu, A. A.; Dezmirean, D. S. The Contribution of Silk Fibroin in Biomedical Engineering. *Insects* **2022**, *13* (3), 286.
- (18) Hong, H.; Seo, Y. B.; Kim, D. Y.; Lee, J. S.; Lee, Y. J.; Lee, H.; Ajiteru, O.; Sultan, M. T.; Lee, O. J.; Kim, S. H.; Park, C. H. Digital light processing 3D printed silk fibroin hydrogel for cartilage tissue engineering. *Biomaterials* **2020**, *232*, 119679.

- (19) Cao, H.; Duan, L.; Zhang, Y.; Cao, J.; Zhang, K. Current hydrogel advances in physicochemical and biological response-driven biomedical application diversity. *Signal Transduction Targeted Ther.* **2021**, *6* (1), 426.
- (20) Zheng, D.; Chen, T.; Han, L.; Lv, S.; Yin, J.; Yang, K.; Wang, Y.; Xu, N. Synergetic integrations of bone marrow stem cells and transforming growth factor- β 1 loaded chitosan nanoparticles blended silk fibroin injectable hydrogel to enhance repair and regeneration potential in articular cartilage tissue. *International wound journal* **2022**, *19* (5), 1023–1038.
- (21) da Silva, C. M.; Reis, R. L.; Corrello, V. M.; Jahno, V. D. The efficient role of sodium alginate-based biodegradable dressings for skin wound healing application: a systematic review. *Journal of Biomaterials Science, Polymer Edition* **2024**, *35* (3), 397–414.
- (22) Abou-Okeil, A.; Fahmy, H. M.; El-Bisi, M. K.; Ahmed-Farid, O. A. Hyaluronic acid/Na-alginate films as topical bioactive wound dressings. *Eur. Polym. J.* **2018**, *109*, 101–109.
- (23) Li, H.; Shen, S.; Yu, K.; Wang, H.; Fu, J. Construction of porous structure-based carboxymethyl chitosan/ sodium alginate/ tea polyphenols for wound dressing. *Int. J. Biol. Macromol.* **2023**, *233*, 123404.
- (24) Ishfaq, B.; Khan, I. U.; Khalid, S. H.; Asghar, S. Design and evaluation of sodium alginate-based hydrogel dressings containing *Betula utilis* extract for cutaneous wound healing. *Front. Bioeng. Biotechnol.* **2023**, *11* DOI: 10.3389/fbioe.2023.1042077.
- (25) Brand, M.; Grieve, A. Prophylactic antibiotics for penetrating abdominal trauma. *Cochrane database of systematic reviews* **2019**, *12* (12), Cd007370.
- (26) Thapa, R. K.; Diep, D. B.; Tønnesen, H. H. Topical antimicrobial peptide formulations for wound healing: Current developments and future prospects. *Acta Biomater.* **2020**, *103*, 52–67.
- (27) Da Silva, J.; Leal, E. C.; Carvalho, E. Bioactive Antimicrobial Peptides as Therapeutic Agents for Infected Diabetic Foot Ulcers. *Biomolecules* **2021**, *11* (12), 1894.
- (28) Deo, S.; Turton, K. L.; Kainth, T.; Kumar, A.; Wieden, H. J. Strategies for improving antimicrobial peptide production. *Biotechnology advances* **2022**, *59*, 107968.
- (29) Xuan, J.; Feng, W.; Wang, J.; Wang, R.; Zhang, B.; Bo, L.; Chen, Z. S.; Yang, H.; Sun, L. Antimicrobial peptides for combating drug-resistant bacterial infections. *Drug resistance updates: reviews and commentaries in antimicrobial and anticancer chemotherapy* **2023**, *68*, 100954.
- (30) Magana, M.; Pushpanathan, M.; Santos, A. L.; Leanse, L.; Fernandez, M.; Ioannidis, A.; Giulianotti, M. A.; Apidianakis, Y.; Bradfute, S.; Ferguson, A. L.; Cherkasov, A.; Seleem, M. N.; Pinilla, C.; de la Fuente-Nunez, C.; Lazaridis, T.; Dai, T.; Houghten, R. A.; Hancock, R. E. W.; Tegos, G. P. The value of antimicrobial peptides in the age of resistance. *Lancet. Infectious diseases* **2020**, *20* (9), e216–e230.
- (31) Abushaheen, M. A.; Muzaheed; Fatani, A. J.; Alosaimi, M.; Mansy, W.; George, M.; Acharya, S.; Rathod, S.; Divakar, D. D.; Jhugroo, C.; Vellappally, S.; Khan, A. A.; Shaik, J.; Jhugroo, P. Antimicrobial resistance, mechanisms and its clinical significance. *Disease-a-month* **2020**, *66* (6), 100971.
- (32) Barlow, G. Clinical challenges in antimicrobial resistance. *Nature microbiology* **2018**, *3* (3), 258–260.
- (33) Ni, J. S.; Min, T.; Li, Y.; Zha, M.; Zhang, P.; Ho, C. L.; Li, K. Planar AIEgens with Enhanced Solid-State Luminescence and ROS Generation for Multidrug-Resistant Bacteria Treatment. *Angew. Chem., Int. Ed. Engl.* **2020**, *59* (25), 10179–10185.
- (34) Zuo, Y.; Kwok, R. T. K.; Sun, J.; Lam, J. W. Y.; Tang, B. Z. Aggregation-Induced Emission Macromolecular Materials for Antibacterial Applications. *Macromol. Rapid Commun.* **2023**, *44* (13), e2300104.
- (35) Kargozar, S.; Baines, F.; Hamzehlou, S.; Hill, R. G.; Mozafari, M. Bioactive glasses entering the mainstream. *Drug Discovery Today* **2018**, *23* (10), 1700–1704.
- (36) Ouyang, S.; Zheng, K.; Huang, Q.; Liu, Y.; Boccaccini, A.R. Synthesis and characterization of rubidium-containing bioactive glass nanoparticles. *Mater. Lett.* **2020**, *273*, 127920.
- (37) Han, L.; Xu, N.; Lv, S.; Yin, J.; Zheng, D.; Li, X. Enhanced In Vitro and In Vivo Efficacy of Alginate/Silk Protein/Hyaluronic Acid with Polypeptide Microsphere Delivery for Tissue Regeneration of Articular Cartilage. *Journal of biomedical nanotechnology* **2021**, *17* (5), 901–909.
- (38) Furukawa, H.; Gándara, F.; Zhang, Y. B.; Jiang, J.; Queen, W. L.; Hudson, M. R.; Yaghi, O. M. Water adsorption in porous metal-organic frameworks and related materials. *J. Am. Chem. Soc.* **2014**, *136* (11), 4369–81.
- (39) Teng, L.; Maqsood, M.; Zhu, M.; Zhou, Y.; Kang, M.; Zhou, J.; Chen, J. Exosomes Derived from Human Umbilical Cord Mesenchymal Stem Cells Accelerate Diabetic Wound Healing via Promoting M2Macrophage Polarization, Angiogenesis, and Collagen Deposition. *Int. J. Mol. Sci.* **2022**, *23* (18), 10421.
- (40) Fang, Z.; Chen, J.; Zhu, Y.; Hu, G.; Xin, H.; Guo, K.; Li, Q.; Xie, L.; Wang, L.; Shi, X.; Wang, Y.; Mao, C. High-throughput screening and rational design of biofunctionalized surfaces with optimized biocompatibility and antimicrobial activity. *Nat. Commun.* **2021**, *12* (1), 3757.
- (41) Hampton, M. B.; Kettle, A. J.; Winterbourn, C. C. Inside the neutrophil phagosome: oxidants, myeloperoxidase, and bacterial killing. *Blood* **1998**, *92* (9), 3007–17.
- (42) Dou, Z.; Li, B.; Wu, L.; Qiu, T.; Wang, X.; Zhang, X.; Shen, Y.; Lu, M.; Yang, Y. Probiotic-Functionalized Silk Fibroin/Sodium Alginate Scaffolds with Endoplasmic Reticulum Stress-Relieving Properties for Promoted Scarless Wound Healing. *ACS Appl. Mater. Interfaces* **2023**, *15* (5), 6297–6311.
- (43) Chen, B.; Zhang, H.; Qiu, J.; Wang, S.; Ouyang, L.; Qiao, Y.; Liu, X. Mechanical Force Induced Self-Assembly of Chinese Herbal Hydrogel with Synergistic Effects of Antibacterial Activity and Immune Regulation for Wound Healing. *Small* **2022**, *18* (21), e2201766.
- (44) Yang, W.; Xu, H.; Lan, Y.; Zhu, Q.; Liu, Y.; Huang, S.; Shi, S.; Hancharou, A.; Tang, B.; Guo, R. Preparation and characterisation of a novel silk fibroin/hyaluronic acid/sodium alginate scaffold for skin repair. *Int. J. Biol. Macromol.* **2019**, *130*, 58–67.
- (45) Atefyekta, S.; Blomstrand, E.; Rajasekharan, A. K.; Svensson, S.; Trobos, M.; Hong, J.; Webster, T. J.; Thomsen, P.; Andersson, M. Antimicrobial Peptide-Functionalized Mesoporous Hydrogels. *ACS Biomaterials Science & Engineering* **2021**, *7* (4), 1693–1702.
- (46) Kang, M.; Zhou, C.; Wu, S.; Yu, B.; Zhang, Z.; Song, N.; Lee, M. M. S.; Xu, W.; Xu, F.-J.; Wang, D.; Wang, L.; Tang, B. Z. Evaluation of Structure–Function Relationships of Aggregation-Induced Emission Luminogens for Simultaneous Dual Applications of Specific Discrimination and Efficient Photodynamic Killing of Gram-Positive Bacteria. *J. Am. Chem. Soc.* **2019**, *141* (42), 16781–16789.